Research Article Vol. 39, No. 4 / April 2022 / Journal of the Optical Society of America B 1141

Journal of the Optical Society of America B

OPTICAL PHYSICS

Design of a sparse array for a one-dimensional non-uniform optical phased array

Kunyang Du,[1,2] Rui Wang,[1,*] Jin Guo,[1] Ruitao Jiang,[1,2] Dongbin Kan,[3] and Yaoyuan Zhang[1,2]

[1]State Key Laboratory of Laser Interaction with Matter, Changchun Institute of Optics, Fine Mechanics and Physics, Chinese Academy of Sciences, Changchun, 130033, China
[2]University of Chinese Academy of Sciences, Beijing, 100049, China
[3]Liaoning Luping Machinery Co, Ltd, Tieling, 112001, China
*Corresponding author: darui9999@163.com

Received 3 January 2022; revised 22 February 2022; accepted 28 February 2022; posted 28 February 2022; published 17 March 2022

To effectively improve the far-field scanning range of an optical phased array (OPA), we propose a genetic algorithm using double fitness functions to optimize the array element arrangement of a one-dimensional non-uniform OPA and simulate a one-dimensional OPA with different array element numbers. The results show that the non-uniform OPA with more array elements exhibits an improved grating lobe suppression effect, and the optimized antenna array pattern exhibits improved comprehensive performance upon employing the double fitness function of grating lobe suppression and beam steering. Considering 128 array elements as an example, the sidemode suppression ratio (SMSR) exhibits a 2.8-dB improvement in the steering process, which verifies the importance of incorporating the novel fitness function of steering optimization. In addition, we further analyze the influence of manufacturing errors such as emission intensity and array position on the SMSR; it is found that the OPA obtained by simulation is sufficiently robust. Our research lays a theoretical foundation for the development of a one-dimensional non-uniform OPA sparse array.

https://doi.org/10.1364/JOSAB.452380

1. INTRODUCTION

With the active development of intelligent systems such as autonomous vehicles, robots, and unmanned aerial vehicles, light detection and ranging (LiDAR) systems have attracted considerable attention as high-performance sensors. The beam-steering device is one of the core components of LiDAR systems. At present, the mainstream technology system of LiDAR still uses a mechanical mechanism for beam steering that can achieve omnidirectional three-dimensional image-information acquisition. However, these mechanical LiDAR systems do not meet the requirements of most future application scenarios owing to stability and cost issues. Optical phased array (OPA) technology based on silicon photonics uses chip-level electronic scanning elements to replace the conventional mechanical mechanism [1,2]. It features the advantages of compact structure, low power consumption, and fast scanning speed. Therefore, a silicon-based OPA is the mainstream technology for realizing beam steering in the future, and has broad application prospects [3–6].

The phased array is a classic concept in the radar field [7]. By controlling the initial phase of each element, a fixed phase difference is established, such that the beam can be coherently superposed in the far field to achieve rotation, offset, and scanning. The operating wavelength of a silicon-based OPA is usually 1550 nm. Limited by the current process level, the element spacing of the OPA is greater than half the wavelength, which leads to the appearance of grating lobes in the far-field pattern. The existence of grating lobes limits the scanning range of the OPA and reduces the energy utilization efficiency. Thus far, the method of eliminating grating lobes through array elements with unequal spacing has been the most common approach [8–11]. Array element optimization is a nonlinear problem. A genetic algorithm [10,12–14] and particle swarm optimization algorithms [15,16] have been used to address this problem. In previous optimization of one-dimensional OPAs, the performance difference between ordered non-uniform spacing and fully random non-uniform spacing has been comparatively studied [15], and the optimization problem of sparse arrays in multi-beam steering has been studied [16]. In the previous optimization of two-dimensional OPAs, the influence of feed distribution [10] and the relationship between wavelength and scanning angle [14] were also studied. However, the existing optimization schemes for non-uniform OPAs are generally applicable for only a far-field pattern under the initial single angle, and optimization of the steering process under one-dimensional large-angle scanning has not been researched yet. However, in practical applications, the steering process leads to an increase in background noise, resulting in single or multiple

high peak noise. The main lobe is difficult to distinguish, which significantly affects the performance of the OPA. This implies that array optimization must consider the steering optimization problem.

In this study, considering the requirements for OPAs in practical engineering applications, our improved genetic algorithm incorporates the angle optimization of the array steering, and adopts a double fitness function that simultaneously considers the grating lobe suppression ratio and steering optimization. Based on this, a one-dimensional non-uniform OPA with a variety of array elements is designed, and the optimization effects of the single and double fitness functions are compared and analyzed. The results show that the array structure obtained by the genetic algorithm with double fitness functions can effectively suppress the grating lobes and reduce background noise during the steering process, which is more suitable for practical applications. In addition, we also analyze the impact of factors such as uneven emission intensity caused by manufacturing errors and changes in the position of the array element on the performance.

2. PRINCIPLE OF OPTICAL PHASED ARRAY

The OPA architecture we studied is shown in Fig. 1(a) and adopts a typical one-dimensional OPA structure [11,17]. Phase control is used to control the steering of only a single axis, whereas the other axis adopts wavelength regulation [18]. Compared with the typical two-dimensional OPA, this method only requires $N+1$ control units, which is far less than the $N \times M$ control units required for two-dimensional OPAs, thereby reducing the complexity of the entire antenna system and simplifying the analysis.

For the above one-dimensional OPA, assuming that its N elements are uniformly arranged, the far-field intensity distribution function $E(\theta)$ of the OPA can be expressed as [2,19]

$$E(\theta) = f(\theta) \sum_{i=0}^{N-1} A_i e^{j\frac{2\pi}{\lambda} id(\sin\theta - \sin\theta_s)}, \tag{1}$$

where $f(\theta)$ is the form factor of a single antenna unit, and the rest are the array factors. A_i, λ, d, θ, and θ_s denote the amplitude of the light emitted by the ith element, optical wavelength, array spacing, observation direction, and beam-scanning angle, respectively. Therefore, the intensity distribution function $E(\theta)$ of the OPA is equal to the product of the form factor of the phased array unit and the array factor, as shown in Fig. 1(b). Furthermore, for the one-dimensional non-uniform OPA we studied, the element spacing d_i is no longer a constant. At this time, to further simplify the analysis difficulty of array optimization, for the far-field model of Eq. (1), it is assumed that the form factor of the array element is isotropic ($f(\theta) = 1$), and the amplitude intensity of the light emitted by each element is equal ($A_i = 1$). Under this condition, the far-field intensity distribution function $E(\theta)$ of the OPA can be expressed as

$$E(\theta) = \sum_{n=1}^{N} e^{j\frac{2\pi}{\lambda}\sum_{i=1}^{n-1} d_i(\sin\theta - \sin\theta_s)}, \tag{2}$$

where di denotes the distance between the ith element and the $(i+1)$th element.

3. IMPROVED DESIGN OF FITNESS FUNCTION

A genetic algorithm is a stochastic global search and optimization method based on biological genetics and evolutionary mechanisms in nature [20]. It searches for the optimal solution by simulating the natural evolution process. The general steps of a genetic algorithm are shown in Fig. 2, including coding, initial population generation, fitness evaluation and testing, selection, crossover, and mutation. For the problem we are studying, we consider the element spacing as the chromosome to produce the initial population, and subsequently simulate the evolutionary process of the population composed of these chromosomes by means of selection, crossover, and variation. Finally, a group of individuals most adapted to the environment, that is, the OPA layout with the smallest sidelobes, is obtained.

The fitness function, the evaluation function, is the criterion used to distinguish the quality of individuals in the group based on the objective function. This is the driving force for the evolution of the algorithm. The OPA is optimized to eliminate grating lobes while maintaining background noise as low as possible; thus, we use the sidemode suppression ratio (SMSR) as a fitness function. However, without considering optimization of the scanning process, the optimized array can ensure the optimal performance only under a single angle. Therefore, we should consider the influence of the steering process on the performance of the OPA in the optimization process to minimize the SMSR variation of the optimized array within the scanning range. Further, to simplify the analysis, we select only

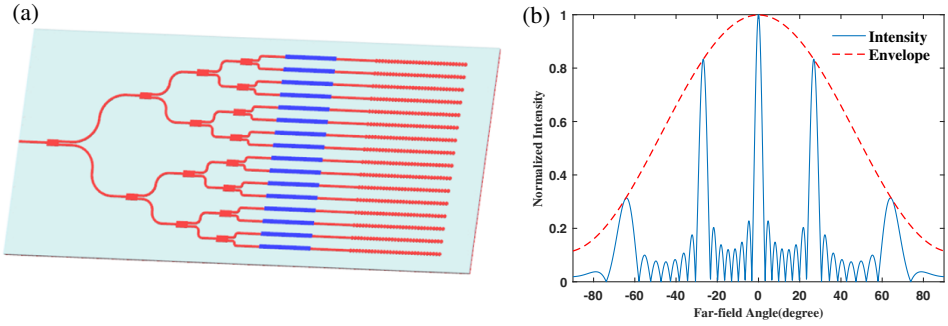

Fig. 1. (a) Schematic of the one-dimensional optical phased array (OPA). (b) Simulated far-field intensity distribution and antenna diffraction envelope for the one-dimensional OPA.

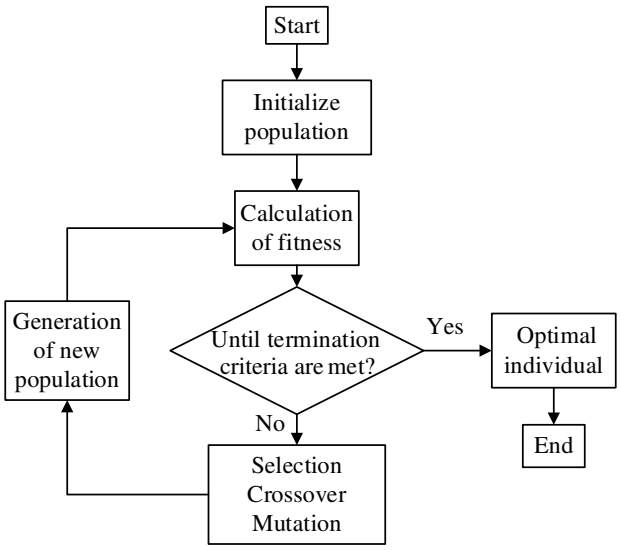

Fig. 2. Flowchart of the genetic algorithm.

the two angles of 0° and the scanning angle θ_s to characterize the scanning process, and add a weight ω to adjust the ratio of the initial SMSR to the scanned SMSR in the optimization process to improve the fitness function. To validate the importance of adding the consideration of steering optimization, two optimization schemes for the fitness function are chosen and compared in this study:

$$\begin{aligned} &\text{Fitness}_1 = \text{SMSR} = 10\lg\left(\frac{I_{\max\text{ sidelobe}}}{I_{\text{mainlobe}}}\right), \\ &\text{Fitness}_2 = \omega_1 \times \text{SMSR}_{\theta=0^\circ} + \omega_2 \times \text{SMSR}_{\theta=\theta_s}, \quad \omega_1+\omega_2 = 1, \end{aligned} \tag{3}$$

where $I_{\max\text{ sidelobe}}$ and I_{mainlobe} represent the maximum power light of the sidelobe and the power of the main lobe, respectively, ω_1 and ω_2 represent the optimized weights of the different steering angles, and $\text{SMSR}_{\theta=0^\circ}$ and $\text{SMSR}_{\theta=\theta_s}$ represent the SMSR at the initial angle and the beam-scanning angle, respectively.

4. SIMULATION OF THE SPARSE ARRAY

A. Simulation of Single Fitness Function

The above genetic algorithm was used to optimize the element of the one-dimensional OPA shown in Fig. 1(a). In the simulation, the operating wavelength was set to 1550 nm, and the optimized range of the element spacing was set to $\lambda - 3\lambda$, considering the influence of coupling between waveguides and the physical size of the antenna, while the emission amplitudes of all elements were assumed to be the same. In addition, to study the influence of the number of array elements on the optimization results, we considered three optimization schemes with different numbers of array elements N, which were set to 16, 64, and 128.

First, the optimization of the single fitness function was considered, and 10 simulations were performed independently for each number of array elements. The best results are shown in Figs. 3–5. It can be seen that, compared with the uniform array, the grating lobes in the far field of the optimized OPA are significantly suppressed, and the suppressed grating lobes energy is dispersed into the sidelobes, increasing background noise. Further analysis shows that the SMSRs of OPAs with the three element numbers are as low as −9.2748, −13.1339, and −14.5023 dB, respectively, when the main beam is not deflected. This trend shows that improved suppression can be realized by increasing the number of elements in the array, significantly reducing the maximum sidelobe level in the far field. We speculate that this is due to the greater freedom of optimization resulting from the increase in the number of elements. From the perspective of the decreasing trend of the SMSR, there is a marginal effect on the optimization effect of the number of elements, and an excessive number of elements cannot result in a rapid decline in the SMSR. In addition, the far-field patterns are also calculated when the beam steering is 30° and 60°. It can be found that as the beam is deflected, the SMSR is increased, but the grating lobe is still in the suppressed state and the main beam can still be clearly distinguished. Thus, the non-uniform OPA overcomes the scanning angle limitation of the periodic array and has the ability to achieve a large scanning range of the field of view.

It is undeniable that our existing simulations are based on the assumption of isotropy of the antenna far-field pattern. However, as shown in Fig. 1(b), the far-field intensity distribution of the OPA must be modulated by the antenna factor. In practical applications, the far-field intensity diffraction envelope of a single antenna cannot be ignored. Furthermore, the changes in the OPA far-field patterns in Figs. 3–5 are analyzed, and the results show that the increase in SMSR is due to the appearance of single or multiple strong sidelobes in the far field after steering, which affects the suppression of the grating lobe. It can be predicted that when the beam is deflected, the energy of these sidelobes will be further enhanced under the influence of the antenna envelope, while the energy of the main lobe will decrease, reducing the contrast between the main beam and sidelobes, thereby affecting the actual performance of the OPA. Considering this situation, in the next optimization process, we add the fitness function of steering optimization to reduce the sidelobes in the steering process and optimize the performance of the OPA.

B. Simulation of Double Fitness Function

In the next simulation, a double fitness function is used. After simulation comparison and analysis, the optimized angle is set to 60°, and the weights ω_1 and ω_2 are 0.6 and 0.4, respectively. The remaining parameter settings are the same as before, and each group of simulation programs is run 10 times randomly. The optimal results obtained are compared with a single fitness function, as shown in Table 1. As shown in the table, under the

Table 1. Comparison of Optimization Results of Different Fitness Functions

Number of Elements	Fitness Function	SMSR (dB)		
		$\theta s = 0°$	$\theta s = 30°$	$\theta s = 60°$
16	Single	−9.2748	−6.4530	−6.4569
	Double	−8.2703	−8.2499	−8.2535
64	Single	−13.1339	−11.2697	−11.1205
	Double	−12.4299	−12.2343	−12.3522
128	Single	−14.5023	−11.4724	−11.5128
	Double	−14.1003	−14.2866	−14.3117

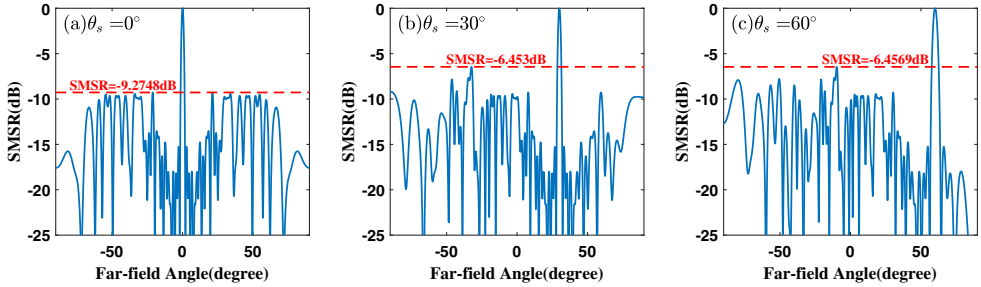

Fig. 3. Sixteen-element OPA far-field intensity distribution optimized using the single fitness function.

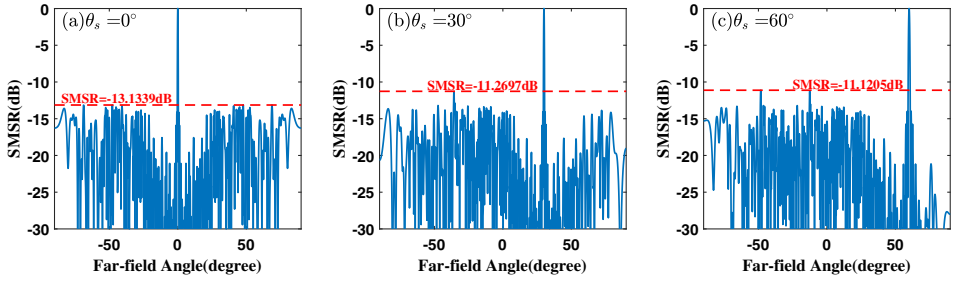

Fig. 4. Sixty-four-element OPA far-field intensity distribution optimized using the single fitness function.

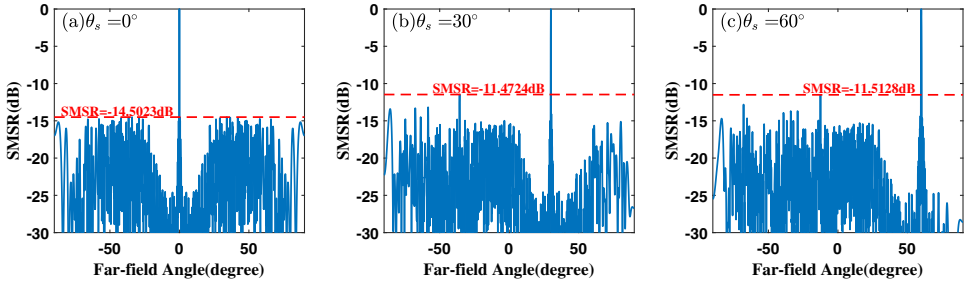

Fig. 5. One-hundred-and-twenty-eight-element OPA far-field intensity distribution optimized with a single fitness function.

optimization of the double fitness function, the SMSR of the OPA of the three array elements deteriorates at 0°, but as the number of array elements increases, the degree of deterioration gradually decreases. When the number of array elements reaches 128, the SMSR is reduced by only 0.4 dB, which is acceptable. Compared with the change in SMSR after the beam is deflected, the SMSR of the double fitness function has a lower change range, and the difference from 0° is approximately 0.2 dB, which improves the performance of the entire steering process. Considering the 128-element OPA as an example, the SMSR of the double fitness function has an improvement of 2.8 dB during the steering process. Figure 6 shows the far-field intensity distribution of the three array elements when the steering angle is 60°. In the figure, the sidelobe intensity distribution is relatively uniform, and there are no prominent sidelobes. Therefore, although the double fitness function cannot guarantee optimal performance in the entire field of view, it trades for an improvement in the steering process at a low cost. Such individuals are more suitable for actual requirements.

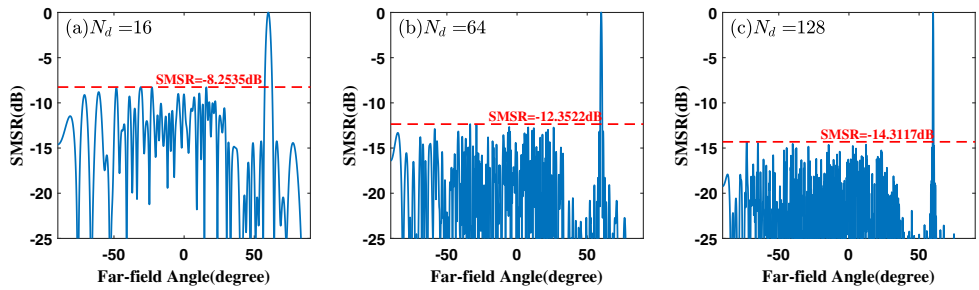

Fig. 6. OPA far-field intensity distribution optimized using the double fitness function, $\theta s = 60°$.

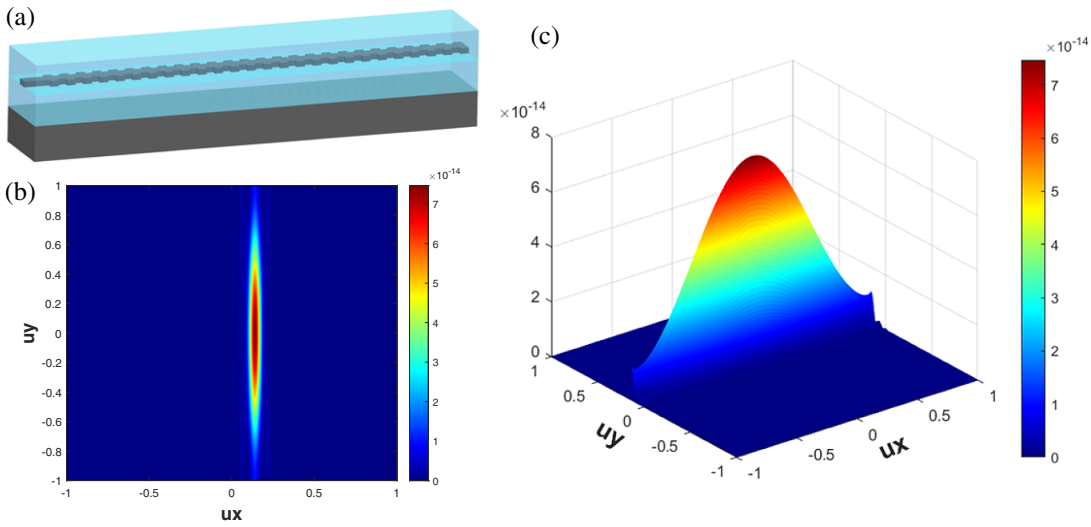

Fig. 7. (a) Schematic of the optical antenna structure. (b) Simulated far-field radiation of the optical antenna. (c) Simulated far-field three-dimensional radiation profile of the optical antenna.

C. Verification

To further verify the importance of considering steering optimization, we discard the assumption that the antenna is isotropic. Instead, we analyze the optimization results of the above two schemes based on the actual situation and the real far-field envelope of the grating antenna. The antenna we used is similar to that mentioned in the literature [3], and its far-field diffraction envelope is obtained by simulation, as shown in Fig. 7. Based on this, the SMSR change curves of the three array elements under the two optimization schemes are calculated, and the overall trend is similar to that of the previous analysis, as shown in Fig. 8. In the case of 0°, the SMSRs of 16 elements are slightly different from the previous simulation results, and the SMSR of the double fitness function is relatively low. We believe that this is related to the intensity distribution after grating lobe suppression, and its sidelobe intensity is located at the lower part of the diffraction envelope. With an increase in the deflection angle, the advantages of the double fitness function gradually manifest. In the single fitness function optimization scheme, when the steering angle of the 16-element reaches 47°, the background noise completely submerges the main lobe. In the double fitness function optimization scheme, the steering range of the 16-element is significantly improved, and the SMSRs of 64 and 128 elements also have improvements of 1.1104 dB and 2.7853 dB, respectively. These results show that the optimization scheme of the double fitness function effectively reduces background noise and improves the actual performance of the OPA in the steering process, which is more meaningful for the design of small array OPAs to realize large-angle scanning. Therefore, it is necessary to incorporate steering optimization to the design process that is more in line with actual application requirements.

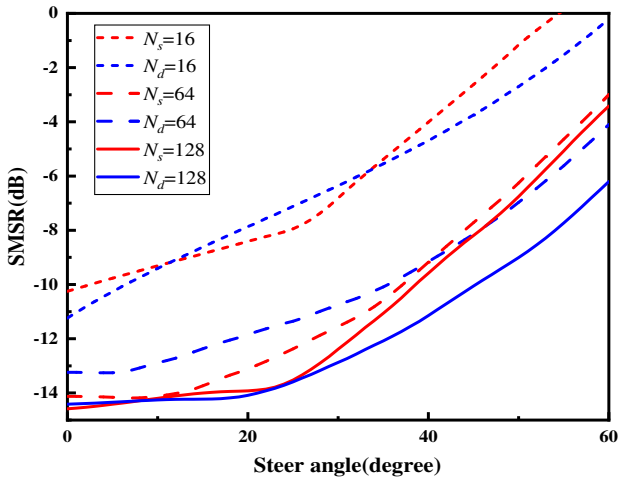

Fig. 8. SMSR curve of OPA optimized using the double fitness function.

5. ERROR ANALYSIS

In addition, we separately study the influence of manufacturing errors, such as the non-uniformity of emission intensity and array position offset on SMSR. Owing to the optimized structure of the unequally spaced array, the optical path of the beam coupled to the antenna is no longer equal for each element. In practice, considering the transmission loss and coupling loss of each device, the amplitude of each element cannot be defaulted to one; therefore, we render an independent random loss ΔA_i to the amplitude of each element. We perform 100 error tests and average the results. The results are presented in Fig. 9(a). It can be found that when the amplitude unevenness is within 10%, the SMSR of the OPA hardly changes, and when the unevenness is up to 40%, the amount of change is still less than 0.5 dB. Similarly, to study the influence of the change in the array position on the performance of the OPA, we assume that the manufacturing error induces a change in the pitch of Δd_i to the pitch of the array. Figure 9(b) shows the results of this change. It can be concluded that there is almost no change in the SMSR within the accuracy of 20 nm, and the SMSR can still maintain a change of less than 0.5 dB within the accuracy of 150 nm. The above analysis shows that non-uniform OPA exhibits high

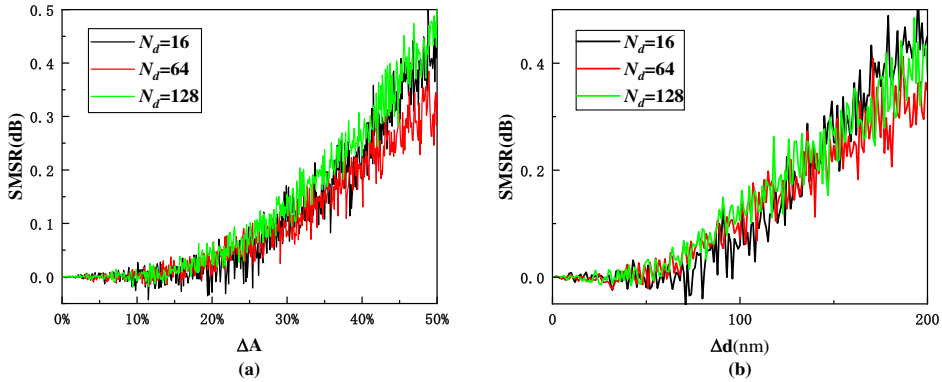

Fig. 9. Investigation of the effect of error: (a) non-uniformity of emission intensity; (b) offset of array position.

robustness, and manufacturing errors have low impact on the performance of the OPA. Interestingly, we found during the research process that manufacturing errors do not cause only deterioration of the SMSR. In some cases, manufacturing errors will instead optimize the SMSR and improve the performance of the OPA.

6. CONCLUSION

In this study, aiming at the grating lobe suppression and steering optimization of OPAs, we use an improved genetic algorithm to design a one-dimensional non-uniform OPA. The results show that the designed OPA can not only effectively suppress the grating lobe, but also reduce background noise in the steering process. Considering 128 array elements as an example, the SMSR is −14.1003 dB at 0° and −14.3117 dB at 60°, thus maintaining appropriate stability over the entire steering range, which is 2.8 dB higher than the result of the single fitness function. The importance of steering optimization in the design of a non-uniform OPA is verified. In addition, within the allowable manufacturing error range, the variation in the SMSR of the designed OPA is less than 0.5 dB, indicating that the array is sufficiently robust. This research on steering optimization could be used as a reference for the design of OPAs in line with practical engineering applications.

Funding. "Xuguang" Talent Program of Changchun Institute of Optics and Machinery, Chinese Academy of Sciences.

Disclosures. The authors declare no conflicts of interest.

Data availability. Data underlying the results presented in this paper are not publicly available at this time but may be obtained from the authors upon reasonable request.

REFERENCES

1. P. F. McManamon, T. A. Dorschner, D. L. Corkum, L. J. Friedman, D. S. Hobbs, M. Holz, S. Liberman, H. Q. Nguyen, D. P. Resler, R. C. Sharp, and E. A. Watson, "Optical phased array technology," Proc. IEEE **84**, 268–298 (1996).
2. S. Jie, E. Timurdogan, A. Yaacobi, S. Zhan, E. S. Hosseini, D. B. Cole, and M. R. Watts, "Large-scale silicon photonic circuits for optical phased arrays," IEEE J. Sel. Top. Quantum Electron. **20**, 264–278 (2014).
3. C. V. Poulton, A. Yaacobi, D. B. Cole, M. J. Byrd, M. Raval, D. Vermeulen, and M. R. Watts, "Coherent solid-state LIDAR with silicon photonic optical phased arrays," Opt. Lett. **42**, 4091–4094 (2017).
4. C. V. Poulton, M. J. Byrd, P. Russo, E. Timurdogan, M. Khandaker, D. Vermeulen, and M. R. Watts, "Long-range LiDAR and free-space data communication with high-performance optical phased arrays," IEEE J. Sel. Top. Quantum Electron. **25**, 7700108 (2019).
5. K. Wang, A. Nirmalathas, C. Lim, E. Wong, K. Alameh, H. Li, and E. Skafidas, "High-speed indoor optical wireless communication system employing a silicon integrated photonic circuit," Opt. Lett. **43**, 3132–3135 (2018).
6. H. W. Rhee, J. B. You, H. Yoon, K. Han, M. Kim, B. G. Lee, S. C. Kim, and H. H. Park, "32 Gbps data transmission with 2D beam-steering using a silicon optical phased array," IEEE Photon. Technol. Lett. **32**, 803–806 (2020).
7. A. Fenn, D. Temme, W. Delaney, and W. Courtney, "The development of phased-array radar technology," Linc. Lab. J. **12**, 321–340 (2000).
8. A. Hosseini, D. Kwong, Z. Yang, C. Yun-Sheng, F. Crnogorac, R. F. W. Pease, and R. T. Chen, "Unequally spaced waveguide arrays for silicon nanomembrane-based efficient large angle optical beam steering," IEEE J. Sel. Top. Quantum Electron. **15**, 1439–1446 (2009).
9. D. N. Hutchison, J. Sun, J. K. Doylend, R. Kumar, J. Heck, W. Kim, C. T. Phare, A. Feshali, and H. Rong, "High-resolution aliasing-free optical beam steering," Optica **3**, 887–890 (2016).
10. R. Fatemi, A. Khachaturian, and A. Hajimiri, "A nonuniform sparse 2-D large-FOV optical phased array with a low-power PWM drive," IEEE J. Solid-State Circuits **54**, 1200–1215 (2019).
11. D. Kwong, A. Hosseini, Y. Zhang, and R. T. Chen, "1×12 Unequally spaced waveguide array for actively tuned optical phased array on a silicon nanomembrane," Appl. Phys. Lett. **99**, 051104 (2011).
12. M. G. Bray, D. H. Werner, D. W. Boeringer, and D. W. Machuga, "Optimization of thinned aperiodic linear phased arrays using genetic algorithms to reduce grating lobes during scanning," IEEE Trans. Antennas Propag. **50**, 1732–1742 (2002).
13. D. Zhang, F. Zhang, and S. Pan, "Grating-lobe-suppressed optical phased array with optimized element distribution," Opt. Commun. **419**, 47–52 (2018).
14. A. Kazemian, P. Wang, Y. Zhuang, and Y. Yi, "Optimization of the silicon-based aperiodic optical phased array antenna," Opt. Lett. **46**, 801–804 (2021).
15. T. Komljenovic, R. Helkey, L. Coldren, and J. E. Bowers, "Sparse aperiodic arrays for optical beam forming and LIDAR," Opt. Express **25**, 2511–2528 (2017).
16. B. Zhang, Y. Liu, Z. Zhao, and P. Yan, "Multi-beam steering with low grating lobes using optimized unequally spaced phased array," Opt. Commun. **427**, 48–53 (2018).
17. K. Van Acoleyen, W. Bogaerts, J. Jágerská, N. Le Thomas, R. Houdré, and R. Baets, "Off-chip beam steering with a one-dimensional optical phased array on silicon-on-insulator," Opt. Lett. **34**, 1477–1479 (2009).
18. D. Kwong, A. Hosseini, J. Covey, Y. Zhang, X. Xu, H. Subbaraman, and R. T. Chen, "On-chip silicon optical phased array for two-dimensional beam steering," Opt. Lett. **39**, 941–944 (2014).
19. S. J. Orfanidis, *Electromagnetic Waves and Antennas* (2002).
20. J. H. Holland, *Adaptation in Natural and Artificial Systems* (1975).